

Article

Characteristics of Deep Coal Reservoir and Key Control Factors of Coalbed Methane Accumulation in Linxing Area

Chuanqi Tao ^{1,2,*} , Yong Li ³, Yanbin Wang ³, Xiaoming Ni ⁴, Xiang Wu ⁵ and Shihu Zhao ³¹ School of Civil Engineering, Liaoning Petrochemical University, Fushun 113001, China² Liaoning Key Lab of Petro-Chemical Special Building Materials, Fushun 113001, China³ College of Geoscience and Surveying Engineering, China University of Mining and Technology, Beijing 100083, China; zhaoshh0310.syky@sinopec.com (S.Z.)⁴ School of Energy Science and Engineering, Henan Polytechnic University, Jiaozuo 454000, China⁵ China United Coalbed Methane Co., Ltd., Beijing 100016, China

* Correspondence: tao666390@126.com

Abstract: Deep coalbed methane (CBM, commonly accepted as >1500 m) has enormous exploration and development potential, whereas the commercial development of deep CBM exploration areas worldwide has been quite limited. The Linxing area, with coals buried approximately 2000 m deep, shows great development potential. Based on a basic geological analysis of structural and hydrodynamic conditions, combining field tests of reservoir temperature and pressure and indoor measurements of maceral composition, proximate analysis, thermal maturity, porosity and permeability, the factors controlling deep CBM accumulations were discussed. The results show that the present burial depth of the No. 8 + 9 coal seam, mainly between 1698 and 2158 m, exhibits a high reservoir temperature (45.0–64.0 °C) and pressure (15.6–18.8 MPa), except for the uplift area caused by the Zijinshan magma event (with coal depth approximately 1000 m). The maximum vitrinite reflectance ($R_{o,max}$) of the coal varies from 1.06% to 1.47%, while the magma-influenced areas reach 3.58% with a relatively high ash content of 31.3% (air-dry basis). The gas content calculated by field desorption tests shows a wide range from 7.18 to 21.64 m³/t. The key factors controlling methane accumulation are concluded from regional geological condition variations. The north area is mainly controlled by structural conditions and the high gas content area located in the syncline zones. The center area is dominated by the Zijinshan magma, with relatively high thermal maturity and a high gas content of as much as 14.5 m³/t. The south area is developed with gentle structural variations, and the gas content is mainly influenced by the regional faults. Furthermore, the groundwater activity in the eastern section is stronger than that in the west, and the hydrodynamic stagnant areas in the western are more beneficial for gas accumulation. The coals vary from 3.35% to 6.50% in porosity and 0.08 to 5.70 mD in permeability; thus, hydrofracturing considering high temperature and pressure should be applied carefully in future reservoir engineering, and the co-production of gas from adjacent tight sandstones also should be evaluated.

Keywords: deep coalbed methane; gas content; CBM accumulations; Linxing area; maceral composition

Citation: Tao, C.; Li, Y.; Wang, Y.; Ni, X.; Wu, X.; Zhao, S. Characteristics of Deep Coal Reservoir and Key Control Factors of Coalbed Methane Accumulation in Linxing Area. *Energies* **2023**, *16*, 6085. <https://doi.org/10.3390/en16166085>

Academic Editor: Pål Østebø Andersen

Received: 22 July 2023

Revised: 10 August 2023

Accepted: 17 August 2023

Published: 21 August 2023



Copyright: © 2023 by the authors. Licensee MDPI, Basel, Switzerland. This article is an open access article distributed under the terms and conditions of the Creative Commons Attribution (CC BY) license (<https://creativecommons.org/licenses/by/4.0/>).

1. Introduction

More than 47.6×10^{12} m³ of coalbed methane (CBM) resources exist worldwide in deep coal seams [1,2]. The total amount of CBM resources (gas in place) in China was estimated to be as much as 36.8×10^{12} m³ in coals buried at a shallower depth than 2000 m, of which 32% (11.9×10^{12} m³) occurs at a depth of 1500–2000 m and 29% (10.6×10^{12} m³) at a depth of 1000–1500 m [3]. Significant CBM resources are buried deeper than 1500 m or 1000 m, and CBM wells in most coal basins range in depth from 100 to 1400 m, such as the Powder River Basin (55–975 m) [4], the Raton Basin (137–1068 m) [5], the San Juan Basin (169–1220 m) [6], the Surat Basin (100–400 m) [7], and the Sydney Basin (650–850 m) [8].

CBM is controlled by a variety of geological factors, for instance structural conditions, hydrology, deposition and subsidence, paleoclimate, and cap rock performance, as well as favorable reservoir pressure and temperatures [9–11]. The present report shows that in shallow areas, the gas content and coal seams have a positive correlation, but beyond a certain depth (critical conversion depth), the gas content of the coal seams tends to reduce as depth increases because of the negative effect of formation temperature on methane adsorption [12]. The activity of faults and the differences between anticline and synclinal structure have different effects on the preservation of CBM [13,14]. The mudstone caprock has good sealing properties; for example, the mudstone-saturated water breakthrough pressure in the Dacheng area is 16–25 MPa, and the gas content of the coal seam is high in thicker muddy cap rock zones [15]. Regarding hydrogeological conditions, there is a strong hydrodynamic condition in the runoff area, the CBM dissipates easily due to hydraulic erosion, and the relatively weak hydrodynamic stagnant zone is conducive to CBM accumulation [16]. In addition, the degree of salinity of groundwater in the stagnant area is higher and easily forms under higher pressure, which is beneficial to CBM accumulation [17].

CBM is a self-generating and self-storing unconventional natural gas whose top and bottom lithology can comprise sandstone, mudstone and limestone. The previous research on CBM reservoirs mainly focused on a depth of less than 1000 m. This is not sufficient to build an understanding regarding deep CBM accumulation forming geological conditions, hydrocarbon accumulation characteristics and other concepts. The state of deep coalbed methane is unclear, the theory of formation and storage is unknown, and the method used to select favorable zones is not yet systematic. The characteristics of deposition, rock formation and the storage of deep coal reservoirs are not well understood, and the in situ storage status is complicated and the storage characteristics are not clear. The present burial depth ranges from approximately 1698 to 2158 m of the No. 8 + 9 (No. 8 and No. 9 coal seams) coal seam, Carboniferous Taiyuan Formation, Linxing area, in the eastern Ordos Basin. Gas content and coal thickness indicated that there is a huge potential for resources in the deep coal seam of the study area. This paper focuses on deep coal reservoirs in the Linxing area, and describes the coal quality, reservoir temperature and pressure, gas content, porosity, and permeability characteristics of deep coal reservoirs. Key factors controlling deep CBM accumulations are discussed carefully, such as the structural condition, hydrodynamic condition, and thermal maturity of coal. Furthermore, the geological conditions of deep CBM determine that special attention should be paid to the high temperature and pressure, hydrodynamic conditions and the properties of coal in future reservoir engineering, as well as the co-production of gas from adjacent tight sandstones.

2. Geological Setting

The Ordos Basin contains many coal, gas and oil resources [18,19]. Linxing area is located in the northeastern Ordos Basin and its tectonic location is the Jinxi flexural fold belt at the eastern Ordos Basin (Figure 1a,b) [20]. The study area is generally a westward dipping monoclinic structure with a gentle formation dip. Affected by the Early Cretaceous tectonothermal events in the North China Plate, a Zijinshan rock mass developed on the eastern side of the Linxing area; the rock body as a whole exhibits alkaline rock characteristics (alkali-rich, Mg-poor and Fe-poor) and reverse faults are developed [21]. The structure of Linxing area is divided into three secondary structural units: diapir structure uplift belt, ring groove belt, and low-amplitude anticlines. The low-amplitude anticlinal zone is controlled by the north–south extruding stress of the northern margin of the Ordos Basin, and some anticline structures with an E–W extension were formed during the Late Paleozoic [22]. The area is far from the northern margin of the basin, so the amplitude of deformation of anticlines is small, but the northern anticlines are generally larger than the southern anticlines. The formation of the trench belt is based on the late Paleozoic fold belt. After the diapirism in Yanshanian, the rock around the diapir structure is affected by the magma uplift and combines with the upward drag of the diapir tectonics

to form a peripheral syncline [23]. The faults in the north are formed by E–W compression stress. They are distributed in two groups in the direction of N–W and N–E, with a short plane extension distance [24].

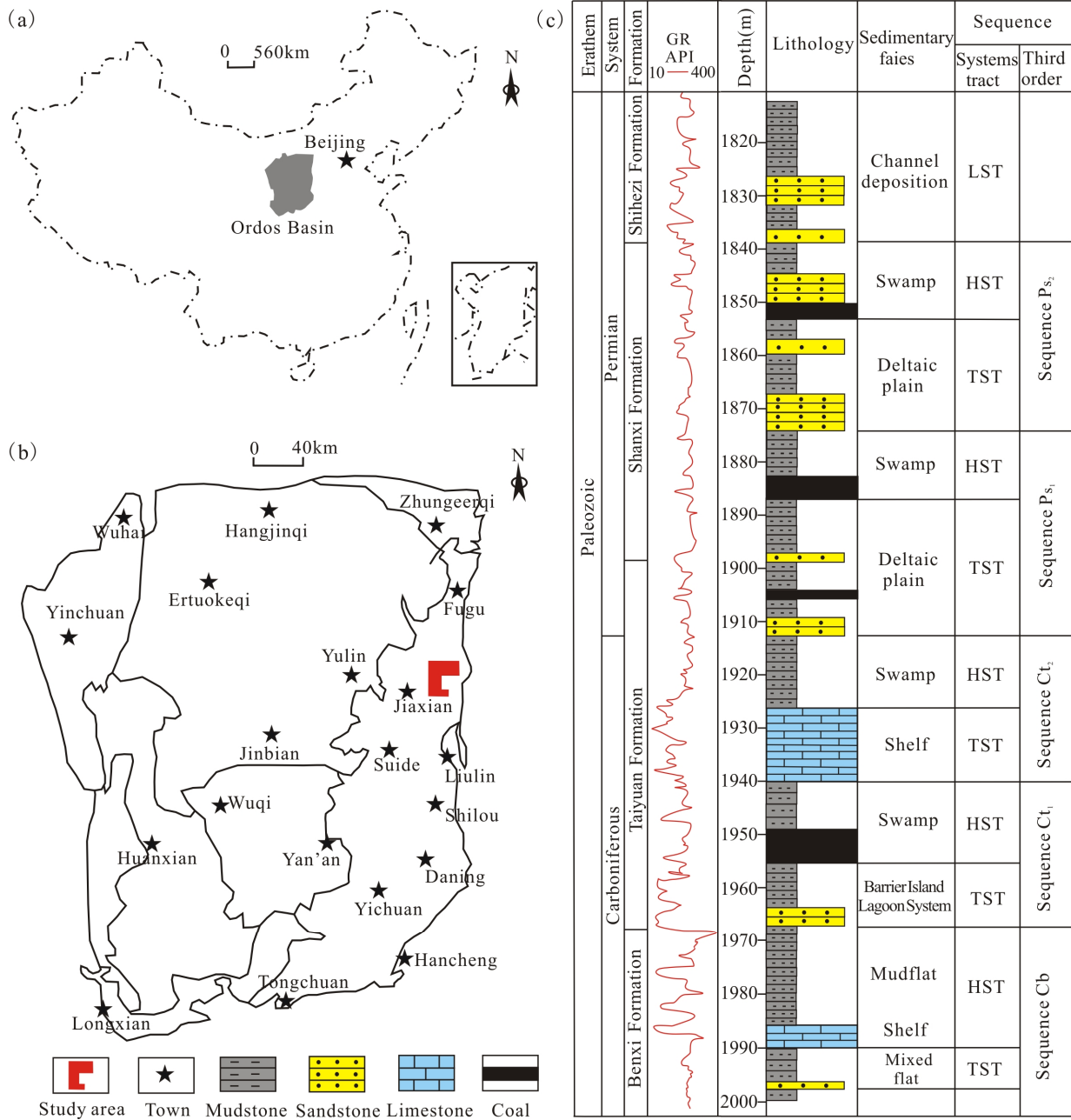


Figure 1. Location of the Linxing area ((a) basin location; (b) study area location in the Ordos Basin) and stratigraphic sequence of the coal-bearing strata (c).

The coal-bearing rock systems in the Linxing area are the Upper Carboniferous–Lower Permian Benxi Formation, Taiyuan Formation and Shanxi Formation. (Figure 1c). There are nine layers of coal seam in this area; among them, the No. 8 + 9 coal seam of Taiyuan Formation is the main coal seam used in the exploration and development of deep CBM [25].

3. Databases and Methods

To describe the properties of deep coal reservoirs in the study area, the coal thickness, burial depth, reservoir temperature, reservoir pressure, in-place gas content, produced water type and total dissolved solids (TDS), and other reservoir geological parameters of the

No. 8 + 9 coal seam were collected from 42 CBM exploration wells. These wells were drilled and data were tested and analyzed by China United Coalbed Methane Co., Ltd. (Beijing, China). The reservoir temperature was measured by logging, and reservoir pressure was obtained from well tests and fracturing tests. The in-place gas content was obtained by the canister tests, according to the method of [26] GB/T19559-2008; Method of determining coalbed gas content. Standardization Administration of the People's Republic of China: Beijing, China, 2008. In addition, in order to reveal the characteristics of deep coal seam, laboratory measurements such as maceral composition analysis, proximate analysis, maturity, maximum pyrolysis temperature, porosity and permeability of coal were carried out.

(1) Maceral composition and vitrinite reflectance of coal

Maceral composition analysis was performed following the China National Standard GB/T 8899-2008. During the test of maceral composition and maximum vitrinite reflectance ($\%R_{o,max}$), the coal rocks were ground to 60–80 mesh, and marked as 30 mm diameter, 10 mm thick coal samples. Statistics and photographs were evaluated for maceral composition. Vitrinite reflectance was performed following China National Standard [27] GB/T 6948-2008; Method of determining microscopically the reflectance of vitrinite in coal. Standardization Administration of the People's Republic of China: Beijing, China, 2008. These tests were performed on the Laborlx 12 POL microscope with the MPS 60 photo system manufactured by the Leitz Company, Oberkochen, Germany.

(2) Maximum pyrolysis temperature and proximate analysis of coal

Following the China National Standard [28] GB/T 18602-2001; Rock pyrolysis analysis. Standardization Administration of the People's Republic of China: Beijing, China, 2001, maximum pyrolysis temperature experiments were performed on coal. The coal samples were crushed and sieved to sample sizes of 0.07–0.15 mm. The experimental instrument was the Rock Eva I6 rock pyrolysis instrument. Proximate analysis of coal was conducted following the China National Standard [29] GB/T212-2008; Proximate analysis of coal. Standardization Administration of the People's Republic of China: Beijing, China, 2008. All coal samples were ground to a particle size of less than 0.2 mm. Approximately 1 g coal samples were placed in a (105–110) °C nitrogen flow drying oven to dry to a constant quality, according to the quality loss of coal samples, to calculate the moisture quality fraction. The volatiles were measured in a covered porcelain crucible and heated at 900 °C for 7 min isolated from air. The reduced quality accounted for the quality fraction of the coal sample quality, with the water content subtracted as the volatile content. The ash content was measured in a muffle furnace. The coal samples were heated to a temperature of 815 °C at a certain rate and burned to a constant mass; the remaining mass accounts for the percentage of coal sample quality as the ash content.

(3) Porosity and permeability of coal

Porosity and permeability tests were performed following the conventional method of the core analysis of the Chinese Oil and Gas Industry Standard [30] SY/T 5336-1996; Method of core routine analysis. China National Petroleum Corporation: Beijing, China, 1996. The samples were cylindrical coal rocks with a length of 3.58–5.34 cm and a diameter of 2.39–2.46 cm. The test conditions were a confining pressure of 300 psi and pore pressure of 200 psi. Porosity was measured using the helium expansion method. Air permeability testing methods were described by Cai et al. [16]. Experimental test data were provided by China University of Mining and Technology.

4. Results

4.1. Burial Depth Variations

The depth of the No. 8 + 9 coal seam ranges from 1698 to 2158 m, with an average value of 1902 m, which is deeper than other typical hydraulic fracture coal seams of coalbed methane basins (Table 1). Regarding the plane distribution, the depth of the coal seam is characterized by the distributions of the “northern is shallow and southwest is deep”. The

north is 1700–2000 m and the south is more than 2000 m (Figure 2). There is a magma uplift region in the central of the study area, which is explained through seismic data. The depth of the coal seam is relatively shallow in the uplift region (e.g., the depth of well L3 is 1090 m).

Table 1. Burial depth of typical hydraulic fracture coal seams of coalbed methane basins.

Basin	Ordos	Qinshui	Piceance	San Juan	Black Warrior	Powder River	Bowen	Sydney
Country	China	China	America	America	America	America	Australian	Australian
Depth (m)	100–1500	200–2000	1560–2561	169–1220	152–1375	55–975	300–1400	650–850
Coal rank	Low-volatile bituminous	Semianthracite to anthracite	Low	Subbituminous A to low-volatile bituminous	Medium–high volatile bituminous	Subbituminous C–A	Medium–high volatile bituminous	High rank (bituminous)

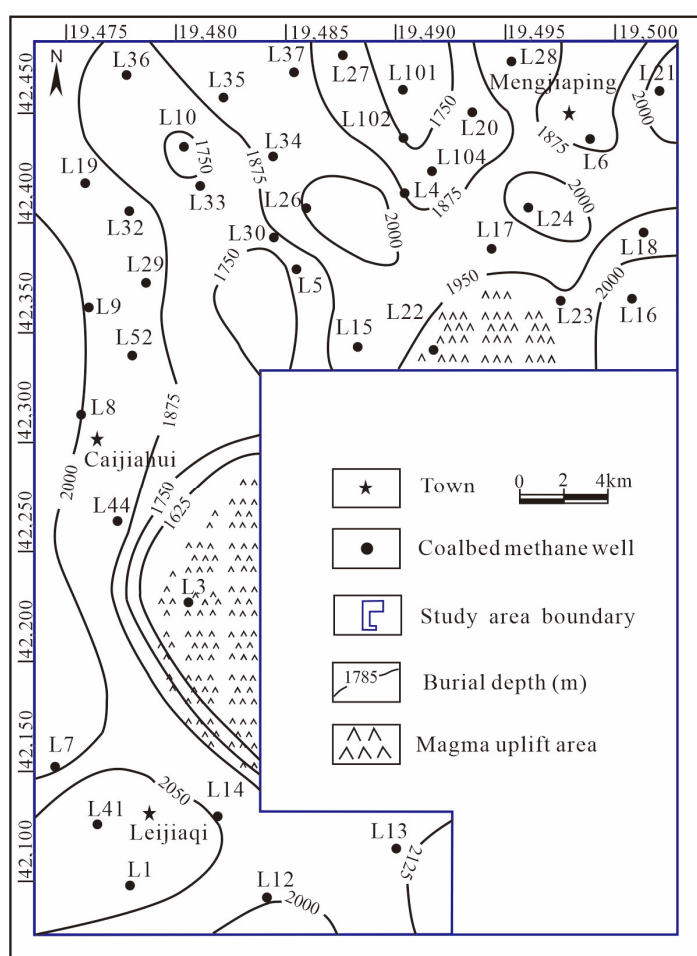


Figure 2. Distribution of depth of the No. 8 + 9 coal seam.

4.2. Material Composition of Coal

4.2.1. Maceral Composition

The maceral composition analysis results indicates that the coals are mainly composed of vitrinite, followed by inertinite, and then, rarely, exinite. The vitrinite is mainly telocollinite and desmocollinite; telinite is occasionally observed (Table 2). The vitrinite content varies from 54.9% to 88.6%, with an average value of 75.6%. The vitrinite content of coals in the south is relatively higher than that in the north. The telinite of well L41 is especially well-preserved (Figure 3), reflecting a rapid deposition and a short gelation time [31]. The inertinite content is between 4.1% and 31.2%, with an average value of 13.9%, which is relatively higher in the north than in the south. The reason for this may be that the source of

the sediment was from the north and the seawater intrusion was mainly from the south and southeast, which led to the fusinitization being stronger in the north than in the south [32].

Table 2. Results of maceral composition and proximate analysis of coals in Linxing area.

Sample No.	Depth(m)	Coal Maceral Composition (%)				Proximate Analysis (%)			
		V	I	E	M	A _d	V _{daf}	M _{ad}	FC _{ad}
L1-1	2086.61	86.2	6.8	0	7.0	12.36	23.34	0.20	64.10
L1-2	2088.16	88.6	8.1	0	3.3	9.73	23.39	0.30	66.58
L1-3	2088.23	86.6	4.1	0	9.3	14.47	23.85	0.25	61.43
L3-1	1068.29	-	-	-	-	31.77	5.99	0.95	61.29
L3-2	1090.14	-	-	-	-	23.81	6.56	0.81	68.82
L4-1	1825.50	75.9	9.8	0	14.3	38.55	24.17	0.40	36.88
L5-1	1769.51	72.9	16.1	0.2	10.8	14.25	27.06	0.40	58.29
L5-2	1770.51	83.6	9.2	0	7.2	11.22	25.79	0.40	62.59
L6-1	1855.64	71.9	17.9	0.2	10.0	23.48	33.67	0.30	42.55
L8-1	1961.80	85.4	5.4	0	9.2	33.17	22.35	0.20	44.28
L18-1	1955.60	-	-	-	-	29.64	7.23	0.26	62.87
L32-1	1936.22	63.7	28.8	0	7.5	21.41	24.36	0.61	53.62
L36-1	1846.29	54.9	31.2	0	13.9	20.26	22.79	1.34	55.61
L36-2	1848.26	62.7	20.7	0	16.6	25.07	25.58	1.50	47.85
L41-1	2158.05	85.2	9.2	0	5.6	18.30	22.50	0.80	58.40

V: vitrinite; I: inertinite; E: exinite; M: minerals; M_{ad}: moisture (air-dry basis); A_d: ash (dry basis); V_{daf}: volatile (dry, ash free basis); FC_{ad}: fixed carbon (air-dry basis).

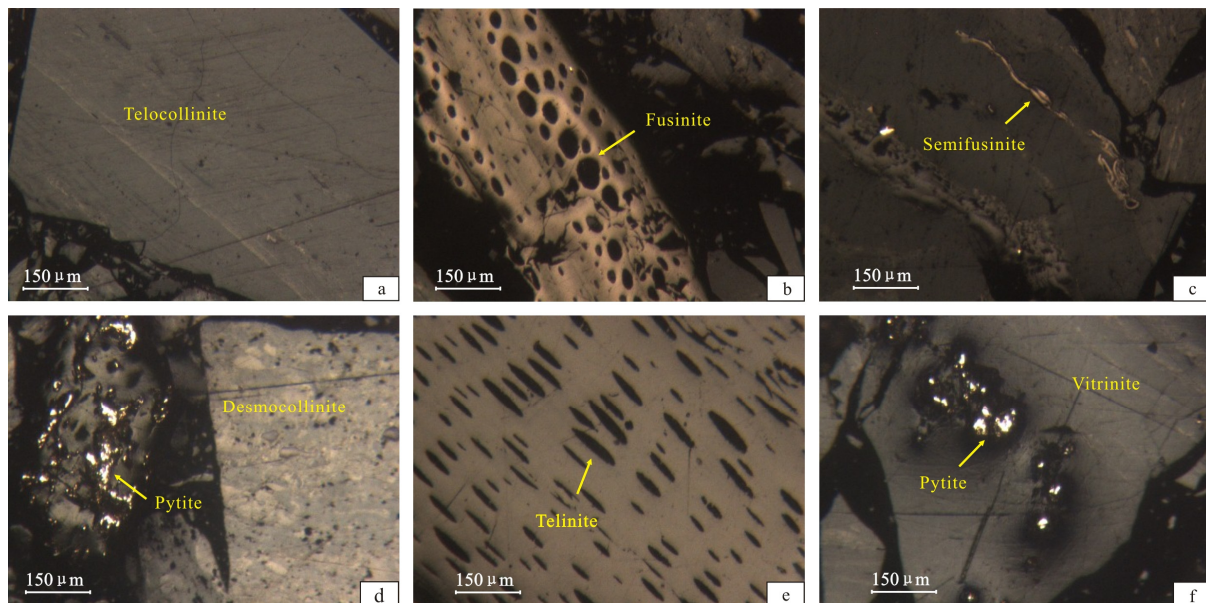


Figure 3. Photos of maceral composition of coal samples from the No. 8 + 9 coal seam in the study area. (a) describes the telocollinite of well L4 (burial depth of 1825.50 m); (b) describes the fusinite of well L5 (1769.51 m); (c) describes the semifusinite of well L8 (1961.80 m); (d) describes the pyrite and desmocollinite of well L35 (1931.20 m); (e) describes the telinite of well L41 (2158.05 m); (f) describes the pyrite and vitrinite of well L52 (2005.00 m).

4.2.2. Proximate Analysis

As shown in Table 2, the water content obtained from the air-dry basis is between 0.2% and 1.5%; the mean value reaches 0.6%. The fixed carbon content ranges from 36.9 to 68.8%; the mean value reaches 55.9%. The volatile content and ash content both show large variation ranges. Most of the coals have a medium-to-low ash content range from 10% to 25%. Ash content is higher near the magma uplift region than it is in other areas.

The magmatic thermal contact increase in coal rank causes the ash content of the coal rock to increase. In addition, the ash content is abnormally high in the northern part of the study area. Because the northern part is the source of sediment, the distributary channel and the tidal channel continuously erode the coal seam in the coal-forming periods [33]. A relatively high content of inorganic minerals existed in the water, which transported and accumulated and precipitated in the coal seam, resulting in higher ash content being found in the coal seam [34].

4.3. Reservoir Pressure and Temperature

4.3.1. Temperature

Stratigraphic temperature influences the adsorption properties of coal, and the ability of coal to absorb methane will decrease as the temperature increases [35,36]. Temperature information is obtained by temperature logging during drilling. Overall, there is a positive correlation between coal reservoir temperature and burial depth. However, this is not a linearly increasing relationship because of the difference in the geothermal gradient (Figure 4). The reservoir temperature is 38.4–64 °C; the mean value is 52 °C. The temperature is higher in the southwestern study area; because of the increased depth of the coal seam, most of the wells exceed 50 °C. The highest temperature was measured in well L1 and well L9, and reached approximately 62 °C. In the magma uplift region, the temperature becomes low because the depth of the coal seams is shallow (e.g., the temperature of well L3 is 38.4 °C) (Figure 5).

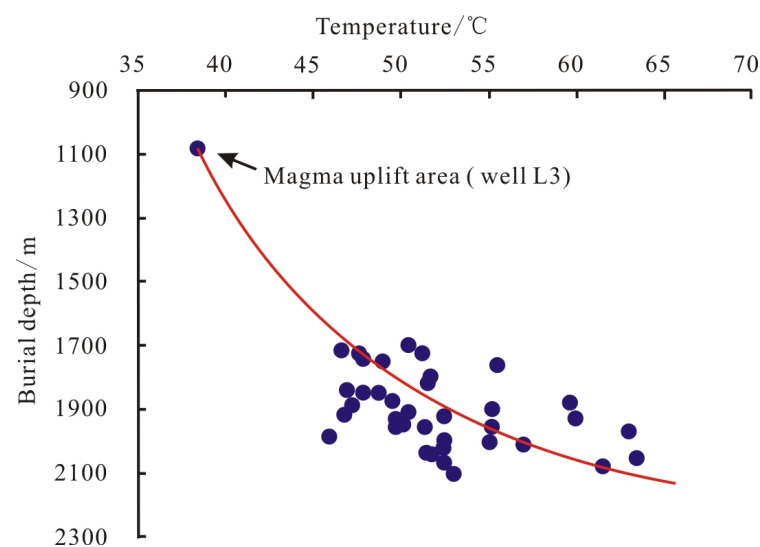


Figure 4. Reservoir temperature versus burial depth of the No. 8 + 9 coal seam.

4.3.2. Pressure

Based on well test reservoir pressure data, the reservoir pressure is 15.6–18.8 MPa, except for the magma uplift region. There is a positive correlation between the reservoir pressure and burial depth; namely, reservoir pressure increases as depth increases (Figure 6a). The reservoir pressure gradient is 0.83–1.02 MPa/100 m, which indicates that the formation is under normal pressure (Figure 6b) [37]. The reservoir pressure gradients are relatively small in the fault development zone and magmatic uplift zone. The location of well L1 is in the syncline area, close to the fault. Well L17 and well L23 are near the Zijinshan uplift zone, where fractures developed. This indicates that the fissure development area may lead to strong differences in gas and water migration, resulting in a decreasing reservoir pressure gradient.

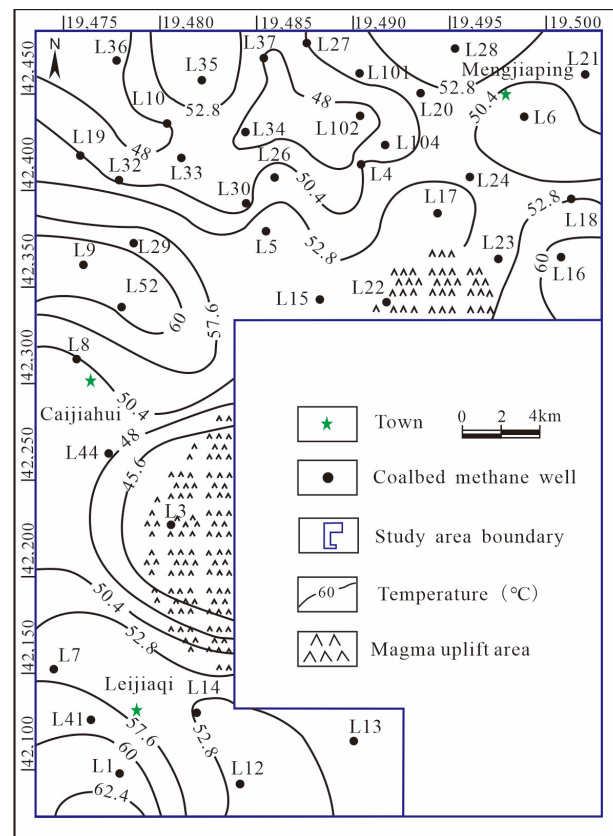


Figure 5. Distribution of temperature of the No. 8 + 9 coal seam.

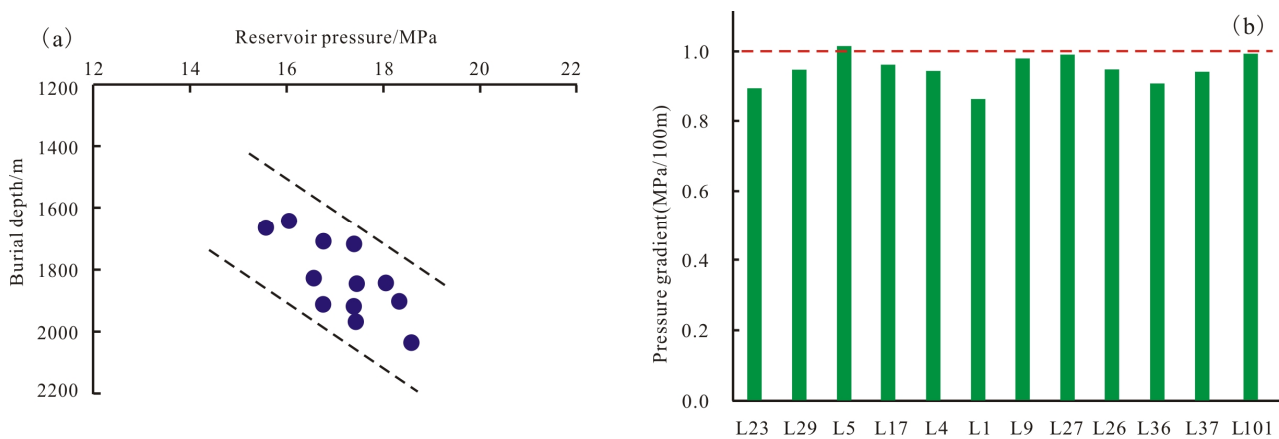


Figure 6. Reservoir pressure versus burial depth (a) and the pressure gradient (b) of the No. 8 + 9 coal seam.

4.4. Thermal Maturity

Coal rank can affect the formation of methane, desorbed gas content and gas storage capacity of coal. In general, the maximum gas storage capacity of coal will increase as coal rank increases. When coal rocks are affected by local heat sources, the gas storage capacity of coal will increase compared with those not affected by heat sources [38].

The measured data show that the maximum vitrinite reflectance ($R_{o,max}$) is from 1.06% to 1.5% of the No. 8 + 9 coal seam. The vitrinite reflectance increases from north to south with the increase in burial depth, but the increasing trend is mild. The vitrinite reflectance clearly increases at the uplift area and, if affected by the Zijinshan magma event, can increase to above 3% (Figure 7).

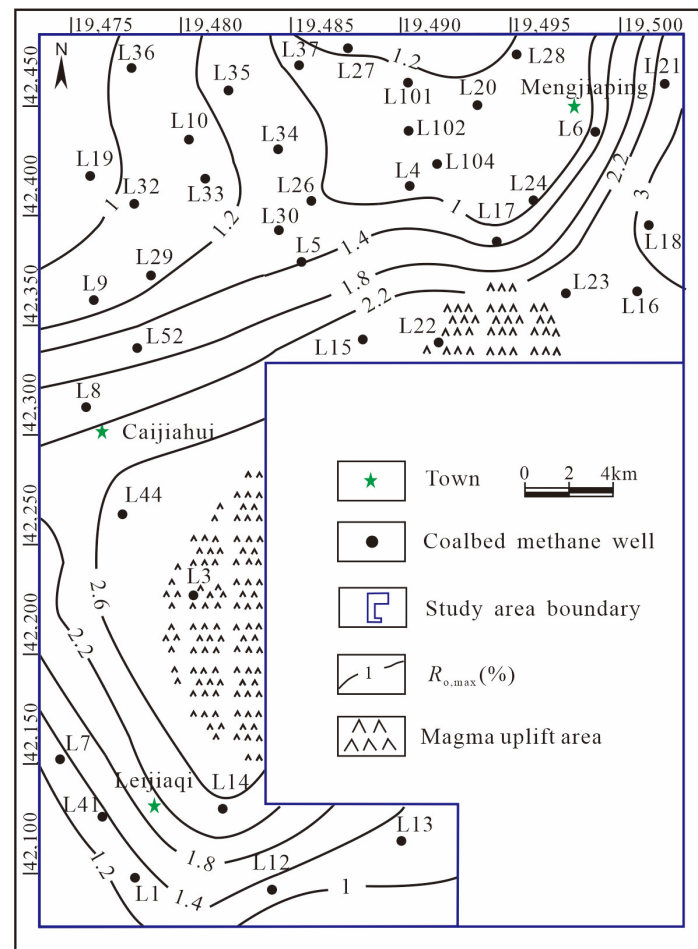


Figure 7. Distribution of coal rank of the No. 8 + 9 coal seam.

4.5. Gas Content and Coal Thickness

Gas content and the thickness of the coal reservoir are important parameters for evaluating CBM resources. The canister tests results show that the gas content is 7.18–21.64 m³/t; the mean value is 12.9 m³/t (Figure 8). The gas content shows a distribution characteristic of “high in west and low in east”. The higher gas content area exceeds 15 m³/t (e.g., well L5, well L6, well L8, and well L32), and the lower gas content area appears in the north (7.18–9.78 m³/t).

The No. 8 + 9 coal seam mainly developed on the intertidal flat, and most of the two coal seams are merged together; only a few coal seams are bifurcated in some areas, due to the change in the sedimentary environment. The thickness of the coal seam ranges from 1.5 to 15.5 m, and the mean value is 5.8 m, which is larger in the south than in the north (Figure 8).

4.6. Characterization of Porosity and Permeability

Due to the lack of tests of permeability in the deep coal seam, the air permeability of coals was tested (Table 3). The test results show that the porosity is 3.35–6.50%, with a mean value of 4.91%, and permeability is 0.08–5.7 mD, with a mean value of 1.69 mD. Compared with previous scholars’ research results, the testing permeability of 55 wells is 0.01–3.33 mD, and the mean value is 0.65 mD in the eastern margin of Ordos Basin [39]; the testing permeability of 7 wells is 0.005–4.94 mD, and the mean value reaches 0.98 mD in the Liulin area of the eastern Ordos Basin [40]. The air permeability of coal in the study area is higher than that of the testing permeability in other areas, but there is no significant difference in the order of magnitude.

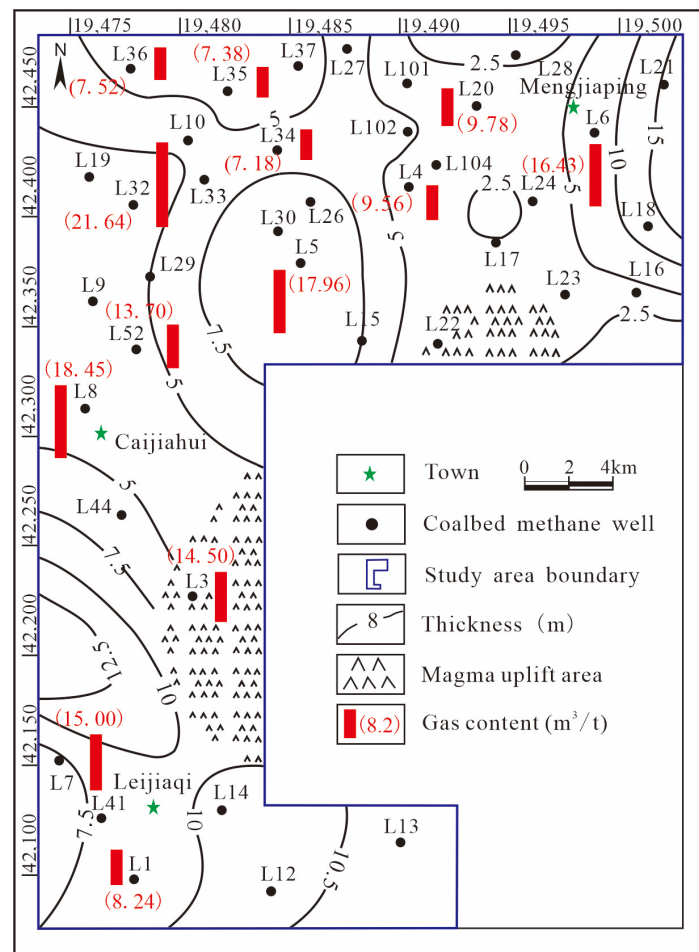


Figure 8. Gas content and thickness of the No. 8 + 9 coal seam.

Table 3. Porosity and permeability of coal samples.

Sample No.	Depth (m)	Length (cm)	Diameter (cm)	Pore Volume (cm ³)	Porosity (%)	Permeability (mD)
L4	1823.0	5.28	2.45	1.25	5.02	0.08
L5-1	1769.2	4.80	2.46	1.24	5.44	2.90
L5-2	1786.0	5.19	2.45	1.41	5.78	0.52
L8	1886.9	3.58	2.44	0.64	4.01	1.95
L10-1	1635.2	4.82	2.43	0.98	4.58	0.26
L10-2	1635.6	5.34	2.39	1.17	4.86	0.20
L15	1895.0	4.54	2.44	1.37	6.50	5.70
L17	1899.0	4.15	2.44	0.96	3.35	1.35
L20	1738.7	4.47	2.44	0.70	4.68	2.21

5. Discussion

5.1. Influences of Structural Patterns on Gas Content

The elevation of the coal seam floor shows large changes in the northern part of the study area, between -720 m and -1000 m (Figure 9b). Overall, the trend is that the east has higher depths relative to the western, which has lower depths. The gas content is clearly controlled by fractures and folds in the northern part of the study area. The gas content is higher in the syncline zone than the anticline zone (Figure 9a). For instance, well L6 is 16.43 m³/t and well L32 is 21.64 m³/t. The gas content is generally small in the anticline zone: well L4 is 9.56 m³/t and well L34 is 7.18 m³/t. One reason for this is that synclinal

reservoirs provide the necessary pressure regimes that are favorable for CBM accumulation, and the syncline zone may be a favorable CBM accumulation area.

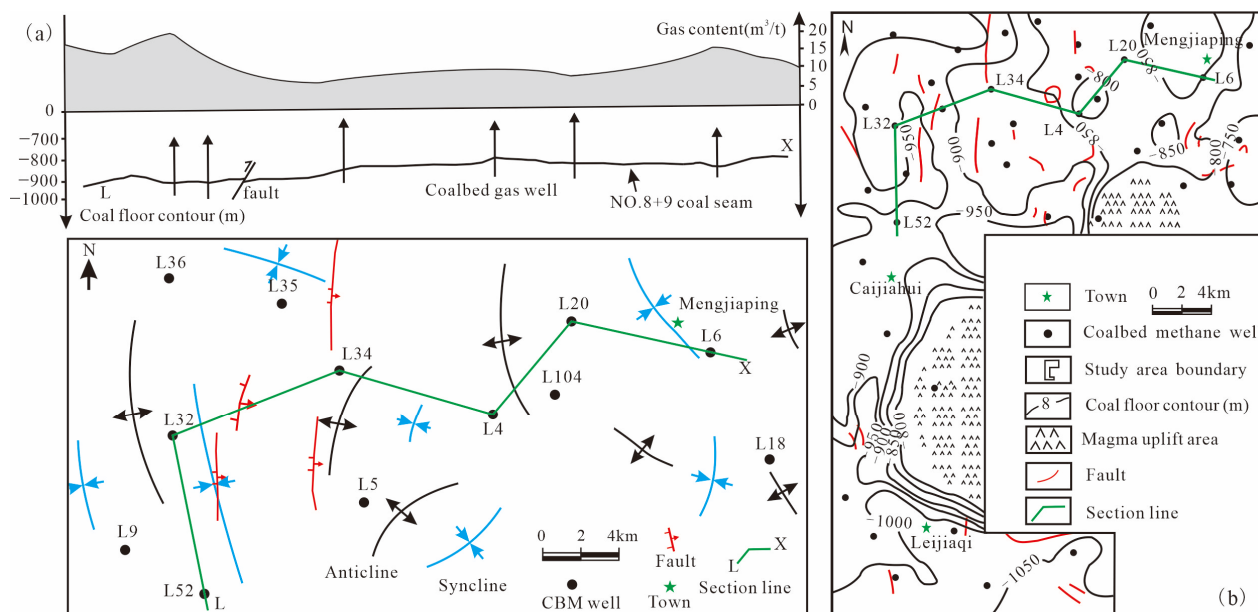


Figure 9. Comprehensive map and cross-section of structure, gas content (a) and coal floor contour (b) in the Linxing area.

The elevation of the coal seam floor is between -1000 m and -1050 m in the southern part, which is relatively flat (Figure 9b). The minor differences in the floor altitude of coal seam have little effect on the accumulation of CBM. However, faults have different kinematic properties, which can affect the distribution of gas content. Well L1 and well L41 are both located in the south of the study area, although there is little difference in the coal quality (the ash content of well L1 is 12.2% and well L41 is 18.3%; the maximum vitrinite reflectance of well L1 is 1.30% and well L41 is 1.47%); the gas content shows large differences (well L1 is 8.24 m³/t and well L41 is 15.0 m³/t). One reason for this may be that well L1 is located on the upthrow side of a reverse fault, which may lead to gas–gas transfer differentiation [41].

5.2. Influences of Hydrodynamic on Gas Content

Based on the data of reservoir pressure and the bottom elevation of the coal seam, the equivalent reduced water level of the study area was calculated using the reduced water-level formula [17]. In the calculation, the sea level is taken as the datum, so the absolute elevation of the datum is taken as 0. The buried depth of No. 8 + 9 coal seam is 1698–2158 m, and the density of water changes very little. Therefore, this can be simplified to calculate the converted head height as $S = 100P + H$, where S is the equivalent reduced water level, m; P is the measured ground pressure, MPa; H is the absolute elevation of the ground pressure test point, m. The results of the calculation are shown in the table below.

The groundwater flow pathway is from east to west, and two groundwater relative stagnant zones are formed: one is in the northwest (well L32, well L8 and well L5) and the other is in the southwest (well L1, well L7) (Figure 10). The gas content of the stagnant area of the groundwater (e.g., well L32 is 21.64 m³/t, well L8 is 18.45 m³/t, well L52 is 13.7 m³/t, and well L41 is 15.0 m³/t) is higher than that of the groundwater runoff area (e.g., well L4 is 9.56 m³/t, well L20 is 9.78 m³/t, and well L34 is 7.18 m³/t). The reason for this is described by Song et al. [14]; the CBM will have a low abundance due to water washing, as some gas may be lost in the runoff zone. In the stagnant zone, water flow is not active, resulting in the preservation of a high abundance of CBM. The groundwater stagnant area may be a favorable area for CBM accumulation.

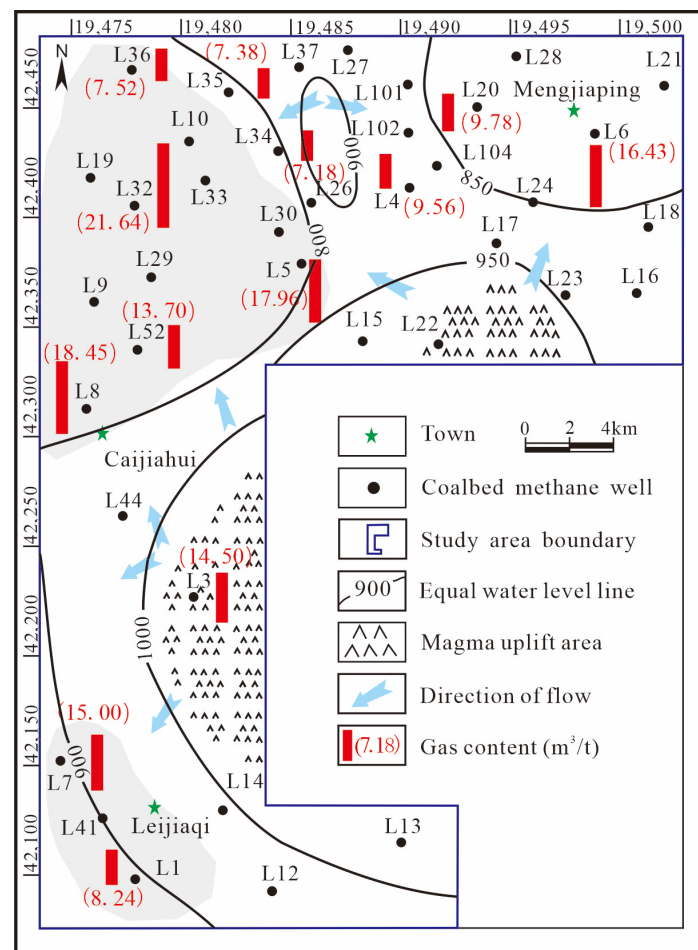


Figure 10. Gas content and hydrodynamics of the No. 8 + 9 coal seam.

The degree of mineralization of groundwater water is an important indicator of the active level of hydrodynamics [42]. Since we did not collect groundwater samples from coal seam, the data collected from formation water showed that the mineralization of groundwater water is very high in the study area. The total dissolved solids (TDS) values were 27,172–48,795 mg/L in the Shanxi Formation, with an average value of 37,975 mg/L; this is 37,026–50,000 mg/L in the Taiyuan Formation, with an average value of 43,513 mg/L. The water type is primarily CaCl_2 , NaCl and Na_2SO_4 .

5.3. Influences of High Reservoir Temperature and Pressure

5.3.1. Variations in Deep Buried Strata

Isothermal adsorption experiment results show that the amount of adsorbed methane decreases with increasing temperature, and this increase in pressure is beneficial for gas adsorption [43,44]. Because of the large burial depth, the temperature and pressure of the deep coal reservoir obviously increase in the deep coal seam when compared to shallow coal seams. Figures 11 and 12 show that when the temperature is less than 50 °C, there is little effect on the gas content. When the temperature exceeds 50 °C, it has a passive influence on the gas content. On the whole, an increase in gas content is accompanied by an increase in reservoir pressure, but this phenomenon is not obvious. A reason for this may be that gas content is significantly affected by structural and hydrodynamic conditions, and the influences of the reservoir temperature and pressure are masked.

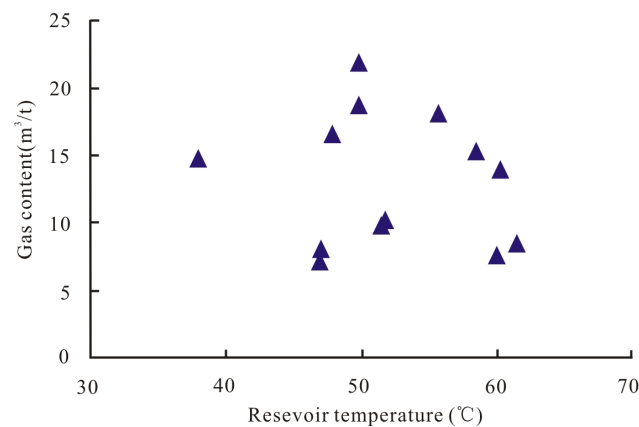


Figure 11. Reservoir temperature versus gas content of the No. 8 + 9 coal seam.

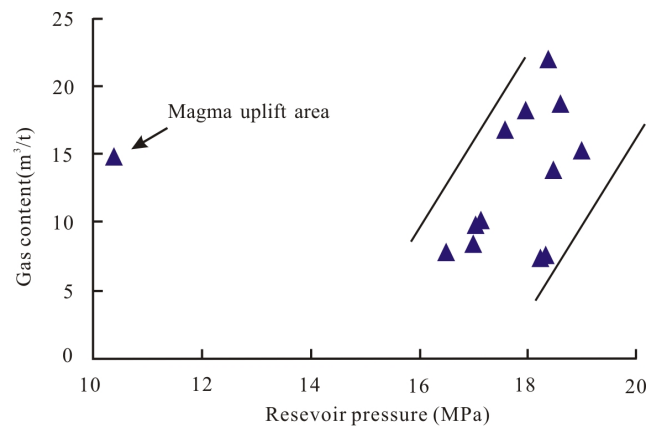


Figure 12. Reservoir pressure versus gas content of the No. 8 + 9 coal seam.

5.3.2. Influences from Magma Event

Magmatic intrusions or volcanic eruptions occurred in the Late Jurassic–Early Cretaceous in Ordos Basin, and the Zijinshan pluton formed during the Yanshanian magmatic intrusion. The results of SHRIMP zircon U–Pb dating, combined with previous research, suggest that the Zijinshan complex was formed between 138.7 Ma and 125.0 Ma, thus belonging to the early Cretaceous epoch [45]. The thermal contact of magma increases the maturity of coal rock, which shows an increasing trend around the Zijinshan, e.g., the vitrinite reflectance of well L3 and well L18 are above 3%. Moreover, the stomatal of coal increase the available space for the adsorption gas of coal, which is beneficial to the adsorption of methane gas for coal rock [46].

To explore the effect of magmatic heat on the coal rock in the vertical direction, the coal samples from L15, L16, L18, and L20 wells, which are relatively close to the magmatic rock mass, were selected for T_{max} analysis. The results show that the T_{max} of coal rocks is 420–600 °C. In the vertical direction, the T_{max} of coals is 450–470 °C in well L15 and well L16, and 450–500 °C in well L20 (Figure 13a,b,d). No abnormally high pyrolysis temperatures occur. The T_{max} of well L18 can reach approximately 600 °C in 1960 m; however, it tends to be normal at the upper and bottom ranges of coal samples (Figure 13c), indicating that the impact of the magma uplift on the coal rock only occurs in a few layers in a vertical direction. The upwelling of deep magma has a distinct influence on the maturity of coal [47].

5.4. Partition of CBM Accumulation

It is generally thought that CBM accumulation is controlled by structural conditions, hydrogeology, sedimentology and coal property [48]. In the Linxing area, CBM accumulation is mainly controlled by structural conditions, hydrogeology and thermal maturity

of coal, and these can be divided into three regions by the floor elevation of coal seams, thermal maturity of coal and gas content, as shown in Figure 14.

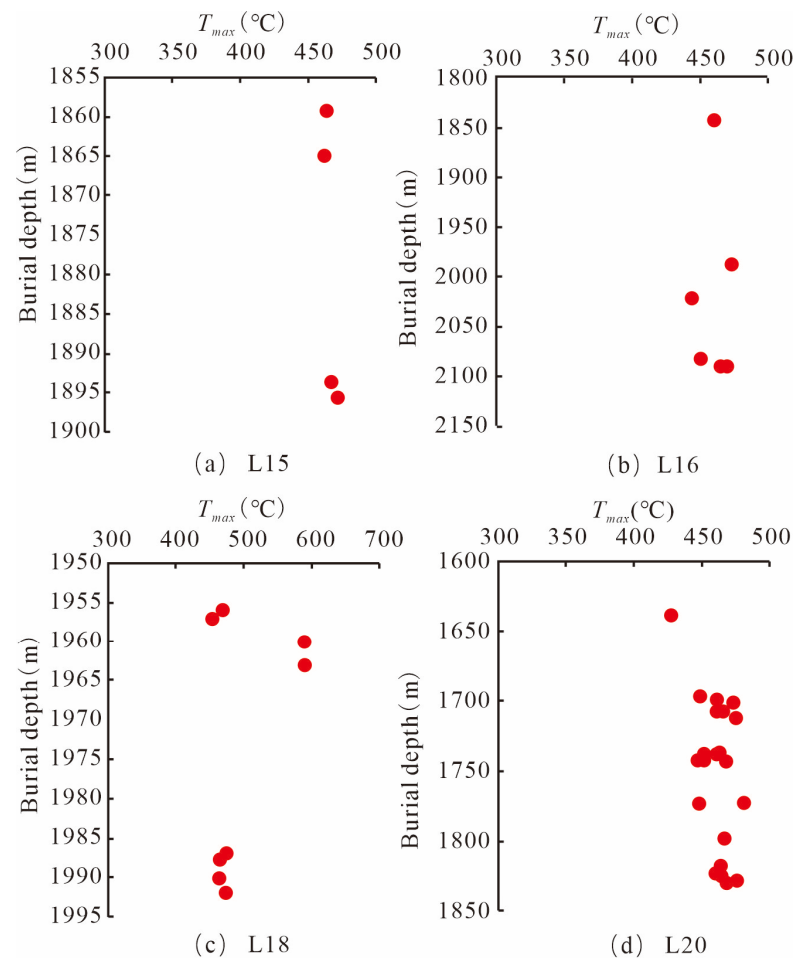


Figure 13. T_{max} of coal versus vertical burial depth in the study area.

Structural condition is the key factor controlling CBM accumulation in the northern part (Region I, shown in Figure 14). The floor elevation of the coal seam shows a large variation range. There is a high gas content (well L6 is $16.43 \text{ m}^3/\text{t}$ and well L32 is $21.64 \text{ m}^3/\text{t}$) in the syncline zones. Nevertheless, the gas content in the anticlinal structure area is generally less than that in syncline zones (well L4 and L34 is $9.56 \text{ m}^3/\text{t}$ and $7.18 \text{ m}^3/\text{t}$, respectively). Due to modern day compressional stresses, the core of the syncline is generally subjected to compressive stress, which generally leads to higher pressure. Furthermore, the syncline zone is generally in the stagnant area of groundwater, which is conducive to the formation of hydraulic plugging gas reservoirs [49,50]. The anticlines and synclines appear alternately from east to the west in the northern part, which leads to the difference in gas content.

For the magma uplift region, shown as Region II, magma causes the formation temperature to increase during geological history, which influences the maturity of coals. The increase in coal rank makes the coal adsorption capacity become stronger; for example, the gas content of well L3 is $14.5 \text{ m}^3/\text{t}$, even when the ash content reaches 30% of the air-dry basis. The direct roof of the coal seam is sandstone with a thickness of 8 m, and it has sand and shale interbedding of a 20 m thickness above the sandstone. Meanwhile, the fractures in the uplift area are relatively developed, which results in some gas escaping to the overlying strata. The gas from adjacent tight sandstones should also be noted.

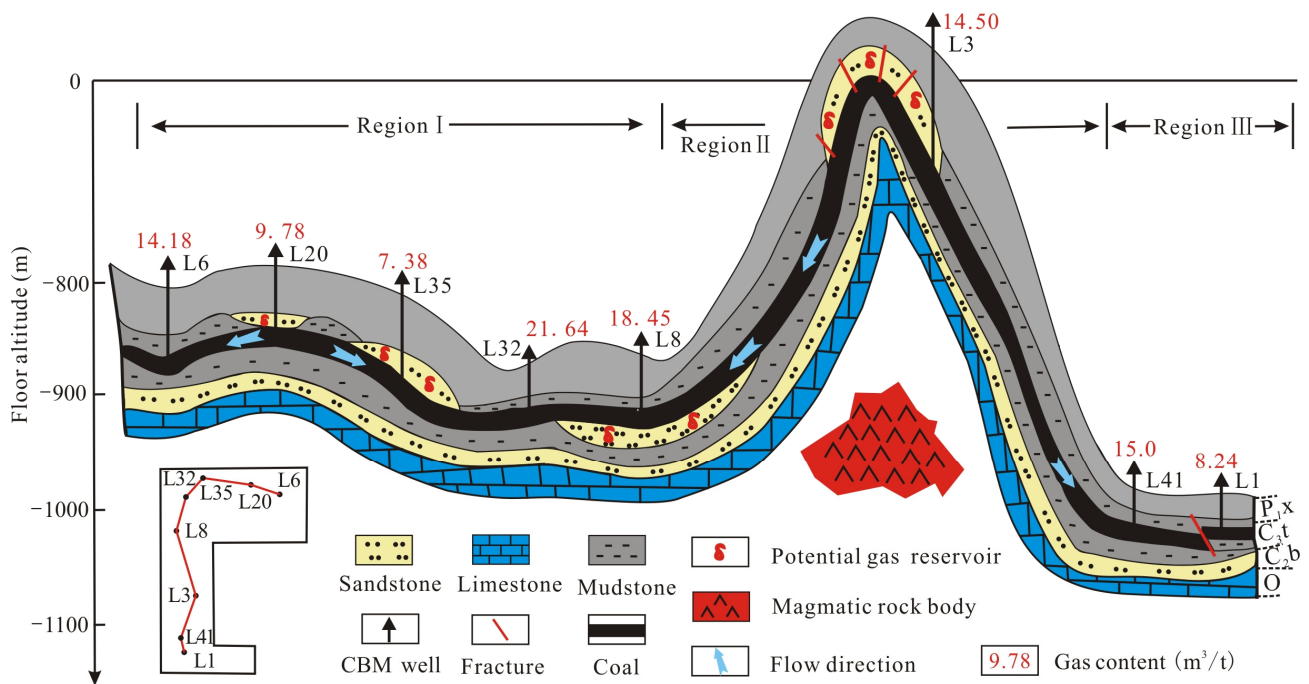


Figure 14. Partition of CBM accumulations in the study area.

The southern part of the study area (Region III) is influenced by coal properties and regional faults. This region is developed, with gentle structural variations, as the elevation of the coal seam floor has few differences (between -1000 m and -1050 m), with a small scale of regional faults. However, the gas content shows great variations. The gas content of well L1 is 8.24 m^3/t , which is lower than the 15.0 m^3/t of well L41. One reason for this is that there is a relatively small difference in the $R_{o,max}$ of coal (well L1 and well L41 are 1.30% and 1.47% , respectively), which leads to the different coal adsorption capacities. Another important reason is that well L1 is located at the upthrown side of the fault, which may lead to some gas dissipation due to stress release. The coal seam is overlaid with shales; this benefits gas preservation.

6. Conclusions

Based on a basic geological analysis of structural and hydrodynamic conditions, combining field and indoor tests, the factors controlling deep CBM accumulation were discussed. For deep buried CBM, several factors should be noted: (1) high reservoir pressure (15.6 – 18.8 MPa) and temperatures (45.0 – 64.0 $^{\circ}\text{C}$); (2) the quite low porosity (from 3.35% to 6.50%) and permeability (from 0.08 to 5.70 mD) of deep coal seams; (3) a wide range of gas content due to different geological backgrounds.

The thickness of the coal seam is 1.5 – 15.5 m, with an average value 5.8 m, along with the gas content of 7.18 – 21.64 m^3/t , indicating a good potential for CBM resources. The structural conditions and thermal maturity of coal are key factors controlling CBM accumulation. The study area can be divided into three regions based on the different key factors controlling the gas content: the north areas by fault/fracture and fold conditions; the middle area by thermal maturity, where the greater the maturity of coal, the larger the gas accumulation; the south area by coal properties and regional faults and fractures.

The effect of stratum temperature on the gas content of deep coal seams needs to be paid attention, while the fracture, fault structure and hydrodynamic conditions of coal have an important influence on the enrichment and escape of coalbed methane.

Author Contributions: Investigation, X.W. and S.Z.; Resources, Y.W.; Data curation, X.N.; Writing—original draft, C.T.; Writing—review & editing, Y.L. All authors have read and agreed to the published version of the manuscript.

Funding: This research was supported by the National Great Science & Technology Specific Project (2016ZX05066001-002, 2017ZX05064-005), National Science Foundation for Young Scientists of China (Grant No. 41702171), Program for Excellent Talents in Beijing (2017000020124G107), Project of Education Department of Liaoning Province (LJKMZ20220744), Doctoral research Start-up Project of Liaoning Petrochemical University (2021XJL-025). We thank China United Coalbed Methane Co., Ltd. and China University of Mining and Technology for providing the data and help for this paper.

Data Availability Statement: The data used to support the findings of this study are included within the article.

Conflicts of Interest: The authors declare no conflict of interest.

References

1. Kuuskraa, V.A.; Wyman, R.E. Deep coal seams: An overlooked source for long-term natural gas supplies. In Proceedings of the SPE Unconventional Resources Conference/Gas Technology Symposium, Calgary, AB, Canada, 3–6 October 1993; Society of Petroleum Engineers: London, UK, 1993; pp. 26–196.
2. Robert, R.T.; Jennifer, L.M. *A conventional Look at an Unconventional Reservoir: Coalbed Methane Production Potential in Deep Environments*; AAPG Annual Convention and Exhibition: New Orleans, LA, USA, 2010; pp. 11–14.
3. Liu, C.L.; Zhu, J.; Che, C.B.; Yang, H.L.; Fan, M.Z. Methodologies and results of the latest assessment of coalbed methane resources in China. *Nat. Gas Ind.* **2009**, *29*, 130–132+152. (In Chinese)
4. Flores, R.M. Coalbed methane in the Powder River Basin, Wyoming and Montana: An assessment of the Tertiary-upper Cretaceous coalbed methane total petroleum system. In *U.S. Geological Survey Digital Data Series DDS-69-C, Version 1*; Department of the interior and Geological Survey: Reston, VA, USA, 2004; Chapter 2; p. 56.
5. Stokes, S.M.; Ge, S.M.; Brown, M.R.M.; Menezes, E.A.; Sheehan, A.F.; Tiampo, K.F. Pore Pressure Diffusion and Onset of Induced Seismicity. *J. Geophys. Res.-Solid Earth* **2023**, *128*. [[CrossRef](#)]
6. Ayers, W.B. Coalbed gas systems, resources, and production and a review of contrasting cases from the San Juan and Powder River Basins. *AAPG Bull.* **2002**, *86*, 1853–1890.
7. Pependick, S.L.; Downs, K.R.; Vo, K.D.; Hamilton, S.K.; Dawson, G.K.W.; Golding, S.D.; Gilcrease, P.C. Biogenic methane potential for Surat Basin, Queensland coal seams. *Int. J. Coal Geol.* **2011**, *88*, 123–134. [[CrossRef](#)]
8. Burra, A.; Esterle, J.S.; Golding, S.D. Horizontal stress anisotropy and effective stress as regulator of coal seam gas zonation in the Sydney Basin, Australia. *Int. J. Coal Geol.* **2014**, *132*, 103–116. [[CrossRef](#)]
9. Tonnsen, R.R.; Miskimins, J.L. Simulation of deep coalbed methane permeability and production assuming variable pore volume compressibility. *J. Can. Pet. Technol.* **2011**, *50*, 23–31. [[CrossRef](#)]
10. Moore, T.A. Coalbed methane: A review. *Int. J. Coal Geol.* **2012**, *101*, 36–81. [[CrossRef](#)]
11. Liu, B.; Chang, S.L.; Zhang, S.; Chen, Q.; Zhang, J.Z.; Li, Y.R.; Liu, J. Coalbed methane gas content and its geological controls: Research based on seismic-geological integrated method. *J. Nat. Gas Sci. Eng.* **2022**, *101*, 104510. [[CrossRef](#)]
12. Qin, Y.; Moore, T.A.; Shen, J.; Yang, Z.B.; Shen, Y.L.; Wang, G. Resources and geology of coalbed methane in China: A review. *Int. Geol. Rev.* **2018**, *60*, 777–812. [[CrossRef](#)]
13. Gurdal, G.; Yalcin, M.N. Gas adsorption capacity of carboniferous coals in the Zonguldak Basin (NW Turkey) and its controlling factors. *Fuel* **2000**, *79*, 1913–1924. [[CrossRef](#)]
14. Song, Y.; Liu, S.B.; Ma, X.B.; Jiang, L.; Hong, F. Favorable depth distribution of coalbed methane enrichment and high yield zone in slope areas. *Acta Geol. Sin.* **2017**, *99*, 371–372. [[CrossRef](#)]
15. Zhang, S.H.; Tang, S.H.; Qian, Z.; Pan, Z.J.; Guo, Q.L. Evaluation of geological features for deep coalbed methane reservoirs in the Dacheng Salient, Jizhong Depression, China. *Int. J. Coal Geol.* **2014**, *133*, 60–71. [[CrossRef](#)]
16. Cai, Y.D.; Liu, D.M.; Yao, Y.B.; Li, J.Q.; Qiu, Y.K. Geological controls on prediction of coalbed methane of No. 3 coal seam in Southern Qinshui Basin, North China. *Int. J. Coal Geol.* **2011**, *88*, 101–112. [[CrossRef](#)]
17. Wang, B.; Sun, F.J.; Tang, D.Z.; Zhao, Y.; Song, Z.H.; Tao, Y. Hydrological control rule on coalbed methane enrichment and high yield in FZ Block of Qinshui Basin. *Fuel* **2015**, *140*, 568–577. [[CrossRef](#)]
18. Tang, X.; Zhang, J.C.; Shan, Y.S.; Xiong, J.Y. Upper Paleozoic coal measures and unconventional natural gas systems of the Ordos Basin, China. *Geosci. Front.* **2012**, *3*, 863–873. [[CrossRef](#)]
19. Zhu, X.M.; Zhong, D.K.; Yuan, X.J.; Zhang, H.L.; Zhu, S.F.; Sun, H.T.; Gao, Z.Y.; Xian, B.Z. Development of sedimentary geology of petroliferous basins in China. *Pet. Explor. Dev.* **2016**, *43*, 820–829. (In Chinese) [[CrossRef](#)]
20. Xie, Y.G.; Qin, Y.; Meng, S.Z.; Pan, X.Z.; Gao, L.J.; Duan, C.J. Study on occurrence characteristics and controlling factors of permian deep coalbed methane in Linxing block. *Fresenius Environ. Bull.* **2022**, *31*, 3408–3414.
21. Xu, H.; Tang, D.Z.; Zhao, J.L.; Li, S. A precise measurement method for shale porosity with low-field nuclear magnetic resonance: A case study of the Carboniferous-Permian strata in the Linxing area. *Fuel* **2015**, *143*, 47–54. [[CrossRef](#)]

22. Shen, J.; Li, K.X.; Zhang, H.W.; Shabbiri, K.; Hu, Q.J.; Zhang, C. The geochemical characteristics, origin, migration and accumulation modes of deep coal-measure gas in the west of Linxing block at the eastern margin of Ordos Basin. *J. Nat. Gas Sci. Eng.* **2021**, *91*, 103965. [[CrossRef](#)]
23. Shen, J.; Zhang, C.J.; Qin, Y.; Zhang, B. Effect factors on co-mining of sandstone gas and coalbed methane in coal series and threshold of parameter in Linxing block, Ordos Basin. *Nat. Gas Geosci.* **2017**, *3*, 479–487.
24. Li, J.; Tang, S.H.; Zhang, S.H.; Li, L.; Jiang, G.W.; Xi, Z.; Sun, K. Characterization of unconventional reservoirs and continuous accumulations of natural gas in the Carboniferous-Permian strata, mid-eastern Qinshui Basin, China. *J. Nat. Gas Sci. Eng.* **2018**, *49*, 298–316. [[CrossRef](#)]
25. Fu, X.Y.; Meng, Y.J.; Li, Z.C.; Kong, P.; Chang, S.L.; Yan, T.T.; Liu, Y.F. Coalbed Methane Potential Evaluation and Development Sweet Spot Prediction Based on the Analysis of Development Geological Conditions in Yangjiapo Block, Eastern Ordos Basin, China. *Geofluids* **2021**, *2021*. [[CrossRef](#)]
26. GB/T19559-2008; Method of Determining Coalbed Gas Content. Standardization Administration of the People's Republic of China: Beijing, China, 2008.
27. GB/T 6948-2008; Method of Determining Microscopically the Reflectance of Vitrinite in Coal. Standardization Administration of the People's Republic of China: Beijing, China, 2008.
28. GB/T 18602-2001; Rock Pyrolysis Analysis. Standardization Administration of the People's Republic of China: Beijing, China, 2001.
29. GB/T212-2008; Proximate Analysis of Coal. Standardization Administration of the People's Republic of China: Beijing, China, 2008.
30. SY/T 5336-1996; Method of Core Routine Analysis. China National Petroleum Corporation: Beijing, China, 1996.
31. Bustin, R.M.; Clarkson, C.R. Geological controls on coalbed methane reservoir capacity and gas content. *Int. J. Coal Geol.* **1998**, *38*, 3–26. [[CrossRef](#)]
32. Xie, X.Y. Provenance and sediment dispersal of the Triassic Yanchang Formation, southwest Ordos Basin, China, and its implications. *Sediment. Geol.* **2016**, *335*, 1–16. [[CrossRef](#)]
33. Jiang, Z.X.; Xu, J.; Wang, G.T. The discovery and significance of a sedimentary hiatus within the Carboniferous Taiyuan Formation, northeastern Ordos Basin, China. *AAPG Bull.* **2012**, *96*, 1173–1195. [[CrossRef](#)]
34. Vassilev, S.V.; Kitano, K.; Vassileva, C.G. Relations between ash yield and chemical and mineral composition of coals. *Fuel* **1997**, *76*, 3–8. [[CrossRef](#)]
35. Zhou, D.; Feng, Z.C.; Zhao, D.; Zhao, Y.S.; Cai, T.T. Uniformity of temperature variation in coal during methane adsorption. *J. Nat. Gas Sci. Eng.* **2016**, *33*, 954–960. [[CrossRef](#)]
36. Pashin, J.C. Stratigraphy and structure of coalbed methane reservoirs in the United States: An overview. *Int. J. Coal Geol.* **1998**, *35*, 207–238. [[CrossRef](#)]
37. Tian, L.; Cao, Y.X.; Chai, X.Z.; Liu, T.J.; Feng, P.W.; Feng, H.M.; Zhou, D.; Shi, B.; Oestreich, R.; Rodvelt, G. Best practices for the determination of low-pressure/permeability coalbed methane reservoirs, Yuwu Coal Mine, Luan mining area, China. *Fuel* **2015**, *160*, 100–107. [[CrossRef](#)]
38. Scott, S.; Anderson, B.; Crosdale, P.; Dingwall, J.; Leblang, G. Coal petrology and coal seam gas contents of the Walloon Subgroup Surat Basin, Queensland, Australia. *Int. J. Coal Geol.* **2007**, *70*, 209–222. [[CrossRef](#)]
39. Zhao, J.L.; Tang, D.Z.; Xu, H.; Li, Y.; Li, S.; Tao, S.; Liu, W.J.; Liu, Z.X. Characteristic of In Situ Stress and Its Control on the Coalbed Methane Reservoir Permeability in the Eastern Margin of the Ordos Basin, China. *Rock Mech. Rock Eng.* **2016**, *49*, 3307–3322. [[CrossRef](#)]
40. Li, Y.; Tang, D.Z.; Xu, H.; Yu, T.X. In-situ stress distribution and its implication on coalbed methane development in Liulin area, eastern Ordos Basin, China. *J. Pet. Sci. Eng.* **2014**, *122*, 488–496. [[CrossRef](#)]
41. Li, M.; Jiang, B.; Miao, Q.; Wang, G.; You, Z.J.; Lan, F.J. Multi-Phase Tectonic Movements and Their Controls on Coalbed Methane: A Case Study of No. 9 Coal Seam from Eastern Yunnan, SW China. *Energies* **2020**, *13*, 6003. [[CrossRef](#)]
42. Chen, S.D.; Tao, S.; Tian, W.G.; Tang, D.Z.; Zhang, B.; Liu, P.C. Hydrogeological control on the accumulation and production of coalbed methane in the Anze Block, southern Qinshui Basin, China. *J. Pet. Sci. Eng.* **2021**, *198*, 108138. [[CrossRef](#)]
43. Yang, M.; Jia, G.N.; Gao, J.L.; Liu, J.J.; Zhang, X.B.; Lu, F.C.; Liu, L.; Pathak, A. Experimental study on the influence of aerated gas pressure and confining pressure on low-rank coal gas adsorption process. *Energy Explor. Exploit.* **2022**, *40*, 381–399. [[CrossRef](#)]
44. Liu, Y.; Zhu, Y.M.; Liu, S.M.; Li, W.; Tang, X. Temperature effect on gas adsorption capacity in different sized pores of coal: Experiment and numerical modeling. *J. Pet. Sci. Eng.* **2018**, *165*, 821–830. [[CrossRef](#)]
45. Wang, Y.Y.; Cai, J.H.; Yan, G.H.; Zhou, W.W.; Yan, Z.J. SHRIMP zircon U-Pb age, geochemistry and Sr-Nd-Hf isotopic characteristics of the Zijinshan alkaline complex in Linxian County, Shanxi Province. *Acta Petrol. Mineralogica* **2014**, *33*, 1052–1072, (In Chinese with English Abstract).
46. Li, K.J.; Chen, G.; Li, W.; Wu, X.L.; Tan, J.C.; Qu, J.W. A comparative evaluation of coal specific surface area by CO₂ and N₂ adsorption and its influence on CH₄ adsorption capacity at different pore sizes. *Fuel* **2016**, *183*, 420–431.
47. Yang, X.K.; Chao, H.X.; Zhang, Z.F.; Yao, W.H.; Dong, M. Characteristics of the Zijinshan complex and its dynamic environment in the east of the Ordos Basin-Analysis of a classic example on the deep processes of the magma activity in the basin. *Geotecton. Metallog.* **2010**, *34*, 269–281.
48. Yao, Y.B.; Liu, D.M.; Yan, T.T. Geological and hydrogeological controls on the accumulation of coalbed methane in the Weibei field, southeastern Ordos Basin. *Int. J. Coal Geol.* **2014**, *121*, 148–159. [[CrossRef](#)]

49. Zhang, Z.G.; Qin, Y.; You, Z.J.; Yang, Z.B. Distribution characteristics of in-situ stress field and vertical development unit division of CBM in western Guizhou, China. *Nat. Resour. Res.* **2021**, *30*, 3659–3671. [[CrossRef](#)]
50. Wang, D.; Nong, C.G.; Zhu, Q.Q.; Wang, P.; Wu, D.; Liu, Z. Study on Geological main controlling factors of CBM enrichment in medium-high rank coal. *Fresenius Environ. Bull.* **2022**, *31*, 8088–8096.

Disclaimer/Publisher’s Note: The statements, opinions and data contained in all publications are solely those of the individual author(s) and contributor(s) and not of MDPI and/or the editor(s). MDPI and/or the editor(s) disclaim responsibility for any injury to people or property resulting from any ideas, methods, instructions or products referred to in the content.